Scripta Materialia 206 (2022) 114229

Contents lists available at ScienceDirect

Scripta Materialia

journal homepage: www.elsevier.com/locate/scriptamat

A new dynamic recrystallization mechanism in adiabatic shear band of an α/β dual phase titanium alloy: Composition redistribution

Xinjie Zhu[a,b,c], Qunbo Fan[a,b,c,*], Duoduo Wang[a,b,c], Haichao Gong[a,b], Yu Gao[a,b], Feng Qian[a], Shenbao Jin[d], Gang Sha[d]

[a] School of Materials Science and Engineering, Beijing Institute of Technology, Beijing 100081, China
[b] National Key Laboratory of Science and Technology on Materials under Shock and Impact, Beijing Institute of Technology, Beijing 100081, China
[c] Beijing Institute of Technology Chongqing Innovation Center, Chongqing 401135, China
[d] Department of Materials Science and Engineering, Herbert Gleiter Institute of Nanoscience, Nanjing University of Science and Technology, 210094, Nanjing, China

ARTICLE INFO

Article history:
Received 24 May 2021
Revised 17 August 2021
Accepted 23 August 2021

Keywords:
Dynamic recrystallization
Adiabatic shear bands
Composition redistribution
Atom probe tomography

ABSTRACT

In this paper, the composition distribution characteristics in adiabatic shear bands (ASBs) of an α/β dual phase Ti-5.5Mo-7.2Al-4.5Zr-2.6Sn-2.1Cr alloy and its influence on dynamic recrystallization (DRX) were investigated via atomic probe tomography. The results showed that in the ASB transition region, a clear grain boundary (GB) in α/β interface was observed. However, in the ASB central region, a "fuzzy GB" was formed in α/β interface, and abundant dislocations accumulated in the "fuzzy GB". In addition, β stabilizing elements (Mo/Cr) became rather sparse in some local regions of β grains to form finer α grains, while in some regions of α grains, local β stabilizing elements were enriched to form finer β grains, thus separating the original grains into finer DRX grains. The unique composition distribution characteristics in α/β grains and α/β interface were defined as composition redistribution, which was the combined result of localized plastic deformation and adiabatic temperature rise.

Adiabatic shear bands (ASBs) are local regions characterized by severe plastic flow due to the plastic instability caused by strain softening of materials, and they often lead to the failure of materials, such as titanium alloys [1-5], steel [6-8], aluminum alloys [9,10], and copper alloys [11,12] under dynamic loading. Moreover, due to a lower thermal conductivity, ASBs are easier to occur in titanium alloys [13]. Therefore, the ASB formation mechanism in titanium alloys has been a promising research field [14, 15].

At present, the researches on ASBs of titanium alloys are usually based on the characterization and analysis of the ASB microstructure [16-19]. Wang et al. [20] investigated the adiabatic shear localization of a β-type Ti-5Al-5Mo-5V-1Cr-1Fe alloy. The results showed that the ASB microstructure consisted of deformed ultrafine grains with high density dislocations. Yang et al. [21] found that the formation of ultrafine grains in ASBs of Ti-1300 alloy was induced by the rotating dynamic recrystallization. In our previous work [22], the microstructure evolution process near ASBs of Ti20C alloy was quantitatively characterized. The results proved that the microstructure softening was the main factor of adiabatic shear failure.

In fact, the microstructure is closely related to the composition distribution characteristics. Prasad et al. [23] investigated the microstructure evolution during the dynamic strain aging of a near α-type 834 titanium alloy and found that the interstitial element segregation was the internal reason of the defects. Gao et al. [24] found that in Ti-9Mo-6W alloy, nano-scale β phase formed in the enrich regions of Mo and W, while lamellar martensite and β phase formed in the poor regions of Mo and W. Han et al. [25] systematically explored the effect of Y on the microstructure of pure titanium and revealed that the Y segregation at grain boundaries (GBs) effectively inhibited the growth of recrystallization grains. The research by Ruzic et al. [26] on Ti-12Mo alloy showed that the Mo segregation eventually resulted in denser ω phase. It can be reasonably inferred that with the significant change of microstructure, the composition of materials is inevitably redistributed, that is, the composition redistribution occurs during the ASB formation. However, the composition redistribution mechanism and its influence on the DRX process are still unclear, and the related researches have been ignored for a long time. Therefore, in this paper, the dynamic compression tests utilizing SHPB was carried out on an $\alpha+\beta$ dual phase Ti-5.5Mo-7.2Al-4.5Zr-2.6Sn-

* Corresponding author at: Beijing Institute of Technology, School of materials science and engineering, 5#223, No.5 Zhong Guan Cun Nan D..., Beijing 100081, China
E-mail address: fanqunbo@bit.edu.cn (Q. Fan).

https://doi.org/10.1016/j.scriptamat.2021.114229
1359-6462/

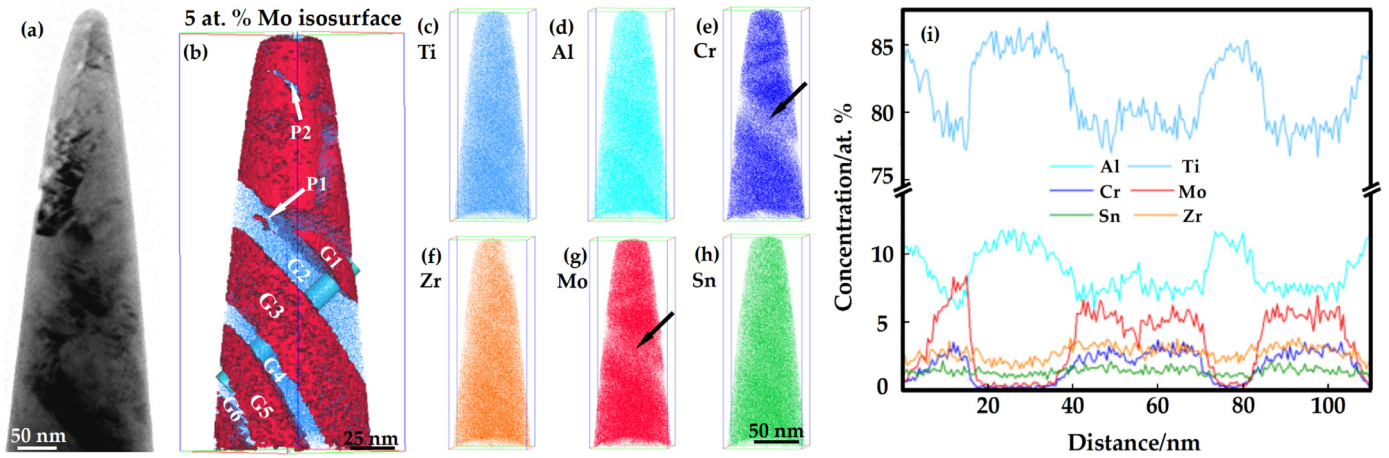

Fig. 1. The microstructure and composition distribution of the transition region. (a) TEM microstructure, (b) 5 at. % Mo isosurface, (c)-(h) three-dimensional composition distribution of alloying elements, and (i) one-dimensional concentration profile along the direction of blue column in (b).

2.1Cr alloy. The composition distribution characteristics near ASBs were quantitatively characterized by focusing ion beam (FIB) and atom probe tomography (APT), and the composition redistribution mechanism and its influence on the DRX process were also investigated.

The as-received material in the present study was an $\alpha+\beta$ dual phase Ti-5.5Mo-7.2Al-4.5Zr-2.6Sn-2.1Cr (wt. %) titanium alloy. The β-transus temperature was determined to be 985 °C±5 °C by metallographic method. The cylindrical specimen with a size of $\varphi 5 \times 5$ mm was machined by wire cutting method, and the dynamic compression tests were carried out on the cylindrical specimen at room temperature and a strain rate of ~3000/s.

APT analysis for 3D element distribution was performed by a CAMECA local electrode atom probe LEAP^{TM} 4000X SI at a target specimen temperature of 40 K, under a pulsing UV laser with a pulse energy of 40-50 pJ, a pulse rate of 200 kHz, and an ion collection rate of 0.6 % per pulse. A tip specimen (apex radius ~50 nm) for APT analyses was prepared by a Zeiss Auriga dual-beam FIB/FEGSEM apparatus using a milling condition of 30 kV and 4 nA for grooving, and a condition of 30 kV and 50-600 pA for ring cutting. The microstructure of the APT specimen was characterized by a FEI-Technai G2 transmission electron microscope (TEM) at 300 kV accelerating voltage. Reconstruction and quantitative analysis of the APT data were conducted on a CAMECA IVAS version 3.6.8 software. The compositions of α phase and β phase were estimated by averaging the core concentrations of the proximity histograms produced by reconstructing 5 at. % Mo isosurface.

The microstructure and three-dimensional composition distribution of the transition region (the micro-deformation region between the ASB central region and the undeformed region, which reflects the parent microstructure and the atom distributions at a certain degree) are shown in Fig. 1. Fig. 1(a) indicates the TEM microstructure of the tip specimen, which shows that inhomogeneous dislocations are distributed in the tip specimen. In fact, due to the quite different element contents between α phase and β phase, most dislocations are distributed in the GB of α phase and β phase. The 5 at. % Mo isosurface of the tip is shown in Fig. 1(b). It indicates that the tip exhibits obvious Mo segregation and is composed of Mo-poor regions and Mo-rich regions with lamellar features. Moreover, the Mo-poor regions and Mo-rich regions distribute almost parallel to each other, separating the tip into six regions marked by symbols of G1-G6. Fig. 1(c)-(h) exhibits the spatial distribution characteristics of Ti, Al, Cr, Zr, Mo and Sn. As shown in Fig. 1(e) and (g), the poor regions of Mo and Cr are clearly distinguished by the arrows. However, significant difference of spatial distribution of Zr and Sn is not observed from Fig. 1(f) and (h).

In order to identify the Mo-poor regions and Mo-rich regions, the average compositions of the typical regions G2 and G3 are obtained and listed in Table 1. The contents of Ti, Al, Cr and Mo in G2 and G3 regions are obviously different. In G2 region, the average content of Al (10.72 at. %) is significantly higher than that in G3 region (7.35 at. %). However, the average contents of Cr (0.30 at. %) and Mo (0.52 at. %) are much lower than that in G3 region (Cr: 3.33 at. % and Mo: 6.79 at. %). Because Al is α stabilizing element, while Cr and Mo are β stabilizing elements. Therefore, G2 and G3 regions are determined as α phase and β phase, respectively. Moreover, it can be further inferred that G4 and G6 regions, which are similar to G2 region, are α phase, and G1 and G5 regions, which are similar to G3 region, are β phase. The average grain size of α and β phases are about 30 nm and 50 nm, respectively. In addition, as shown in Fig. 1(i), the one-dimensional concentration profile along the blue column in Fig. 1(b) is obtained and clearly indicates the distribution characteristics of alloying elements, which also supports the inference about G1-G6 regions.

Furthermore, as shown by the white arrows in Fig. 1(b), Mo-rich region P1 in α grain and Mo-poor region P2 in β grain are found. Particularly, according to the composition distribution characteristics, a distinguishable α/β GB is observed, which is related to the slight plastic deformation of the transition region.

The microstructure of the ASB central region is shown in Fig. 2, in which Fig. 2(a) and (b) are the dark field and bright field images, respectively. It indicates that there are a lot of ultra-fine α and β grains in ASBs, as shown by the short white arrows. According to the annular diffraction pattern in Fig. 2(b), these ultra-fine grains are determined as DRX grains (α_{DRX} and β_{DRX}). Moreover, by comparing the characteristics of the bright regions in Fig. 2(a) with that of the dark regions in Fig. 2(b), it can be found that most of the dark regions in the viewing regions are due to the accumulated dislocations which distributed in the interface of DRX and deformed grains, as shown by the long white arrows. While in some local regions, the dark regions in Fig. 2(b) may be induced by the diffraction contrast, as marked by the yellow dotted lines, because no corresponding bright regions are observed at the same locations in Fig. 2(a).

The microstructure and three-dimensional composition distribution of the ASB central region are shown in Fig. 3. Fig. 3(a) indicates the TEM microstructure of the tip specimen, in which most of the dark regions are due to the high density dislocations, while

Table 1
The average compositions of G2 and G3 regions (at. %)

Region	Ti	Al	Zr	Mo	Cr	Sn	O	Si	C	Fe
G2	82.693	10.72	2.18	0.52	0.30	1.47	0.36	0.041	0.022	0.066
G3	78.673	7.35	2.55	6.79	3.33	1.30	0.53	0.089	0.019	0.084

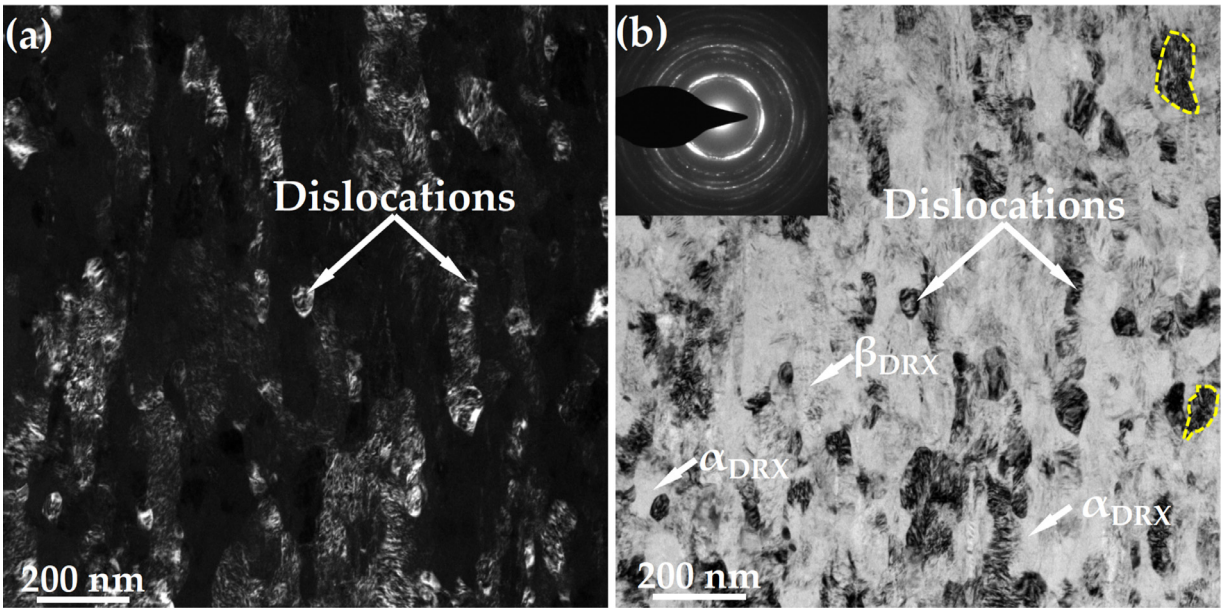

Fig. 2. The microstructure in the ASB central region. (a) The dark field image, (b) the bright field image.

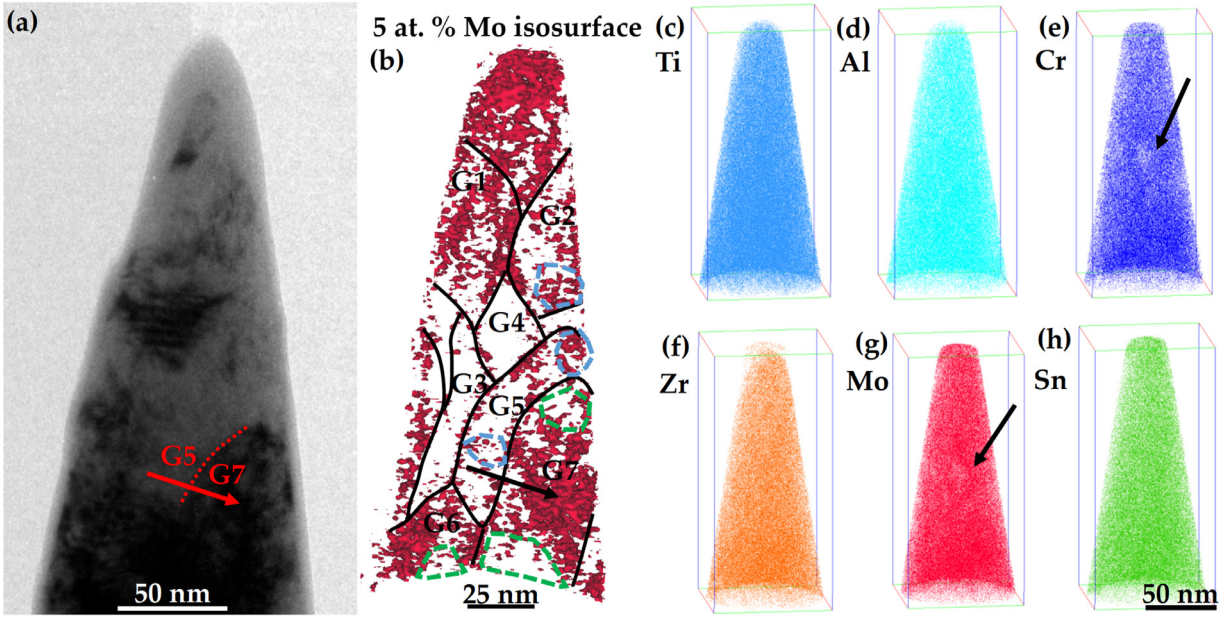

Fig. 3. The microstructure and composition distribution of the ASB central region. (a) TEM microstructure, (b) 5 at. % Mo isosurface, and (c)-(h) three-dimensional composition distribution of alloying elements.

a small part of the dark regions are due to the diffraction contrast. By comparing the composition distribution of 5 at. % Mo isosurface with the TEM microstructure, the tip specimen can be separated into different sub-regions marked by symbols of G1-G7, as shown in Fig. 3(b). Moreover, Mo segregation is also observed in ASBs, and the distribution characteristics of the accumulated dislocations are substantially consistent with that of the Mo segregation. Moreover, as shown in Fig. 3(e) and (g), Mo and Cr show the similar segregation characteristics.

In order to identify the Mo-poor regions and Mo-rich regions, the average compositions of different regions in Fig. 3(b) are obtained and listed in Table 2. The element contents in various regions are obvious different. In G2-G5 regions, the content of Al is higher (more that 9.30 at. %) than that in G1, G6 and G7 regions (less than 8.73 at. %). However, the contents of Mo and Cr are much lower (Mo: less than 2.65 at. % and Cr: more than 1.53 at. %) than that in G1, G6 and G7 regions (Mo: more than 3.54 at. % and Cr: more than 1.89 at. %). Therefore, it can be determined

Table 2
The average contents of alloying elements in different regions (at. %).

Region	Ti	Al	Zr	Mo	Cr	Sn	O	Si	C	Fe
bulk	80.35	8.98	3.08	3.46	1.72	1.31	0.74	0.08	0.06	0.08
G1	81.02	8.61	2.89	3.54	1.97	1.25	0.32	0.10	0.04	0.10
G2	81.50	9.63	3.07	2.65	1.53	1.24	0.17	0.11	0.01	0.01
G3	81.88	9.30	2.98	2.57	1.48	1.21	0.28	0.10	0.02	0.07
G4	83.31	10.43	2.85	1.22	0.71	1.12	0.19	0.07	0.01	0.04
G5	81.87	9.62	2.87	2.36	1.53	1.16	0.33	0.04	0.08	0.08
G6	80.40	8.73	3.24	3.82	1.89	1.31	0.28	0.05	0.10	0.07
G7	78.97	8.33	3.24	5.07	2.49	1.28	0.27	0.07	0.09	0.10

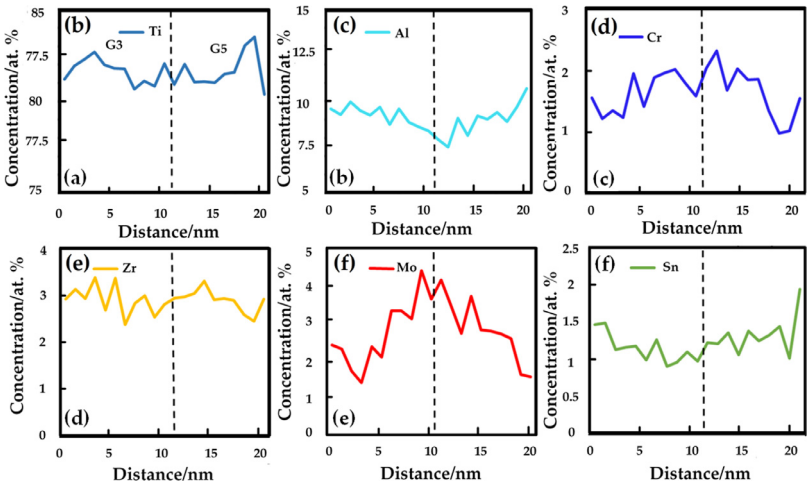

Fig. 4. One-dimensional concentration profiles along the direction of black arrow in Fig. 3(b) showing the composition variations near the GB of G5 and G7.

that G2-G5 regions are α phase while G1, G6 and G7 regions are β phase.

By comparing Fig. 3 with Fig. 2, an obvious difference between the microstructure of the ASB transition region and that of the ASB central region is observed. As shown in Fig. 3, the average grain sizes of α_{DRX} (20 nm) and β_{DRX} (40 nm) in the ASB central region are relatively small, and the grain length is only about 1/3 of that in the ASB transition region shown in Fig. 2. It indicates that grains in the ASB central region exhibit an obvious equiaxed trend. Particularly, in the ASB central region, obvious compositional difference is observed in the interior of α grains or β grains, as shown in Fig. 3(b), indicating the occurrence of the composition redistribution during the ASB formation, which promotes the DRX process. It illustrates a new DRX mechanism in ASBs. In the green dotted boxes in Fig. 3(b), β stabilizing elements (Mo/Cr) in some interior local regions of β grains become sparse to form finer α_{DRX}. Similarly, in some regions of α grains, local β stabilizing elements are enriched to form finer β_{DRX}, as shown in the blue dotted boxes in Fig. 3(b), thus separating the original grains into finer DRX. Moreover, due to the severe deformation and the composition redistribution in the ASB central region, the distribution characteristics of the accumulated dislocations are substantially consistent with that of the element segregation.

Furthermore, the composition distribution characteristics near the GB in the ASB central region shown in Fig. 3(b) are very different from that in the transition region shown in Fig. 2(b). In the ASB central region, an indistinguishable “fuzzy GB” is formed in the α/β GB, as shown in Fig. 3(b). Particularly, it is further found that high density dislocations are accumulated in the typical "fuzzy GB" between G5 and G7 regions, as shown in Fig. 3(a).

In order to reveal the composition distribution characteristics in the α/β GB, one-dimensional concentration profiles near the G5/G7 GB along the black arrow in Fig. 3(b), i.e. the red arrow in Fig. 3(a), are obtained and shown in Fig. 4, and the α/β GB is depicted as the dotted line. As shown in Fig. 4(a) and (b), the contents of Ti and Al decrease gradually with a small range. Moreover, as shown in Fig. 4(c)-(e), the contents of Cr, Zr and Mo increase marginally. As shown in Fig. 4(f), the content of Sn is almost unchanged. In summary, the change of element contents in the α/β GB is very limited, which is not consistent with the theoretical one. It illustrates that a new region is formed in the α/β GB, i. e. the “fuzzy GB” mentioned above, where α stabilizing elements and β stabilizing elements are uniformly distributed due to the composition redistribution. During the ASB formation, α stabilizing elements in α grains and β stabilizing elements in β grains migrate to the α/β GB to form the “fuzzy GB”. Actually, the “fuzzy GB” will not keep stability in the subsequent deformation process because of the high density dislocations shown in Fig. 3(a) and the particular composition distribution characteristics shown in Fig. 4, and it will develop into new GBs of DRX grains.

During the ASB formation, β_{DRX} in α grains, α_{DRX} in β grains and the “fuzzy GB” are formed through the composition redistribution, which illustrates a new DRX mechanism in ASBs.

Recent researches indicate that the DRX in ASBs stems from the fact that the dislocations accumulate in local regions to form sub-grain boundaries and eventually develop into new GBs [2, 27-29]. Significantly, the present study further attributes the internal reason of DRX to the composition redistribution. During the dynamic deformation, the localized temperature rises rapidly to more than 1000 °C [2, 17, 30], which promotes the migration of alloying elements [31-33]. In addition, severe deformation makes the dislocation density increase sharply, which may directly lead to the formation of element-poor regions or element-rich regions. Therefore, the compositional difference induced by the element migration and the severe deformation promotes the nucleation of new α grains and new β grains. In the α/β GB, the "fuzzy GB" is filled

with high density dislocations and will develop into new GBs of DRX grains, which promotes the DRX process.

In addition, high density dislocations are accumulated in the "fuzzy GB", which will induce the initiation of micro-cracks for the deformation incompatibility between surrounding regions, and finally leads to adiabatic shear failure.

In this paper, the composition distribution characteristics near ASBs of an α/β dual phase Ti-5.5Mo-7.2Al-4.5Zr-2.6Sn-2.1Cr alloy were quantitatively characterized by APT, and the composition redistribution, a new DRX mechanism in ASBs, was found. The results showed that in the ASB transition region, a distinguishable α/β GB was observed. However, in the ASB central region, an indistinguishable “fuzzy GB” with high density dislocations formed in the α/β interface. Moreover, it was found that β stabilizing elements in some interior local regions of β grains became sparse to form finer α grains; while in some regions of α grains, local β stabilizing elements were enriched to form finer β grains, thus separating the original grains into finer DRX grains. Further research indicated that the unique composition distribution characteristics in α grains, β grains and the α/β interface were caused by the composition redistribution, which was the combined result of localized plastic deformation and the induced adiabatic temperature rise during the dynamic deformation.

Data availability

The raw/processed data required to reproduce these findings cannot be shared at this time due to legal or ethical reasons.

Declaration of competing interest

The authors declare that they have no known competing financial interests or personal relationships that could have appeared to influence the work reported in this paper.

Acknowledgments

This work was financially supported by the Natural Science Foundation of Chongqing (Grant No. Cstc2020jcyj-msxmX0094). In addition, Dr. Xuehao Zheng from ZKKF(Beijing) Science and Technology Co., Ltd was acknowledged for TEM tests and data analysis.

References

[1] B. Huang, X.F. Miao, X. Luo, Y.Q. Yang, Y.M. Zhang, Mater. Charact. 151 (2019) 151–165.
[2] C.K.C. Lieou, C.A. Bronkhorst, Int. J. Plasticity 111 (2018) 107–121.
[3] Q. Li, Y.B. Xu, M.N. Bassim, Mat. Sci. Eng. A 358 (2003) 128–133.
[4] Y.Z. Guo, Q.C. Ruan, S.X. Zhu, Q. Wei, J.N. Lu, B. Hu, X.H. Wu, Y.L. Li, J. Mech. Phys. Solids 135 (2020) 103811.
[5] S.C. Liao, J. Duffy, J. Mech. Phys. Solids 12 (1998) 2201–2231.
[6] M.C. Jo, S. Kim, D.W. Suh, S.S. Hong, H.K. Kim, S.S. Sohn, S. Lee, Mat. Sci. Eng. A 792 (2020) 139818.
[7] M.C. Jo, S. Kim, D.W. Kim, H.K. Park, S.S. Hong, H.K. Kim, H.S. Kim, S.S. Sohn, S. Lee, J. Alloy. Compd. 845 (2020) 155540.
[8] K.C. Le, T.M. Tran, J.S. Langer, Scripta Mater 149 (2018) 62–65.
[9] X.D. Wu, L.X. Li, W.H. Liu, S.K. Li, L. Zhang, H. Hong, Mat. Sci. Eng. A 732 (2018) 91–98.
[10] D.H. Li, Y. Yang, T. Xu, H.G. Zheng, Q.S. Zhu, Q.M. Zhang, Mat. Sci. Eng. A 527 (2010) 3529–3535.
[11] S.B. Yiadom, N. Bassim, Mat. Sci. Eng. A 711 (2018) 182–194.
[12] L. Tang, Z.Y. Chen, C.K. Zhan, X.Y. Yang, C.M. Liu, H.N. Cai, Mater. Charact. 64 (2012) 21–26.
[13] D. Rittel, Z.G. Wang, Mech. Mater. 40 (2008) 629–635.
[14] S.L. Semiatin, T.R. Bieler, Metall. Mater. Trans. A 32A (2001) 1871–1875.
[15] B.K. Kad, S.E. Schoenfeld, M.S. Burkins, Mat. Sci. Eng. A 322 (2002) 241–251.
[16] H.L. Yang, D.D. Wang, X.J. Zhu, Q.B. Fan, Mat. Sci. Eng. A 759 (2019) 203–209.
[17] S.L. Liu, Y.Z. Guo, Z.L. Pan, X.Z. Liu, E.J. Lavernia, Y.T. Zhu, Q.M. Wei, Y.H. Zhao, J. Mater. Sci. Technol. 54 (2020) 31–39.
[18] Y.P. Zheng, W.D. Zeng, Y.B. Wang, D.D. Zhou, X.X. Gao, J. Alloy. Compd. 708 (2017) 84–92.
[19] S.X. Zhu, Y.Z. Guo, Q.C. Ruan, H.S. Chen, Y.L. Li, D.N. Fang, Int. J. Mech. Sci. 171 (2020) 105401.
[20] B.F. Wang, X.Y. Wang, Z.Z. Li, R. Ma, S.T. Zhao, F.Y. Xie, X.Y. Zhang, Mat. Sci. Eng. A 652 (2011) 287–295.
[21] Y. Yang, F. Jiang, B.M. Zhou, X.M. Li, H.G. Zheng, Q.M. Zhang, Mat. Sci. Eng. A 528 (2011) 2787–2794.
[22] X. Liu, Y. Zhou, X.J. Zhu, D.D. Wang, Q.B. Fan, Mat. Sci. Eng. A 746 (2019) 322–331.
[23] K. Prasad, S. Amrithapandian, B.K. Panigrahi, V. Kumar, K.B.S. Rao, M. Sundararaman, Mat. Sci. Eng. A 638 (2015) 90–96.
[24] J.H. Gao, J. Nutter, X.G. Liu, D.K. Guan, Y.H. Huang, D. Dye, W.M. Rainforth, Nat. Commun. 8 (2018) 7512.
[25] G.K. Han, H.K. Park, H.K. Kim, T.S. Jun, Mat. Sci. Eng. A 779 (2019) 139137.
[26] J. Ruzic, S. Emura, X. Ji, I. Qatanabe, Mat. Sci. Eng. A 718 (2018) 48–55.
[27] V.F. Nesterenko, M.A. Meyers, J.C. LaSalvia, M.P. Bonder, Y.J. Chen, Y.L. Lukyanov, Mat. Sci. Eng. A 229 (1997) 23–41.
[28] J.E. Bailey, P.B. Hirsch, Proc. R. Soc. Lond. 267A (1962) 11–30.
[29] W.Q. Guo, J.X. Liu, J. Yang, S.K. Li, Mat. Sci. Eng. A 528 (2011) 6248–6252.
[30] Y. Zhou, Q.B. Fan, X. Liu, D.D. Wang, X.J. Zhu, K. Chen, J. Mater. Sci. Technol. 59 (2020) 138–148.
[31] J.X. Wen, R. Cao, Y.F. Gao, Acta Mater 194 (2020) 276–282.
[32] C. Lei, Y. Zhou, H.X. Zhai, Z.Y. Huang, W.Q. Hu, L.P. Cai, Y.B. Wang, Q. Yu, H.J. Wang, Ceram. Int. 47 (2021) 16422–16431.
[33] S.N. Liu, H.T. Shen, J.W. Xu, X.J. Zhou, J.F. Liu, Z.Y. Cai, X.J. Zhao, L.R. Xaio, J. Mater. Sci. Technol. 81 (2021) 117–122.